ESAIM: PROCEEDINGS, February 2007, Vol.16, 133-145
Eric Cancès & Jean-Frédéric Gerbeau, Editors
DOI: 10.1051/proc:2007016

EVALUATION OF DETACHED EDDY SIMULATIONS FOR PREDICTING THE FLOW OVER PERIODIC HILLS

Šarić, S.[1], Jakirlić, S., Breuer, M., Jaffrézic, B., Deng, G., Chikhaoui, O., Fröhlich, J., von Terzi, D., Manhart, M. and Peller, N.[2]

Abstract. The performance of an hybrid LES–RANS strategy, the Detached Eddy Simulation (DES), as a predictive tool for turbulent channel flow with massive separation is scrutinized. This is undertaken in a collaborative effort involving five different flow solvers used by five different groups to cover a broad range of numerical methods and implementations. This paper concentrates on DES results obtained with a computational mesh of approximately one million cells. The results are compared to those obtained by Large Eddy Simulations (LES) using the standard and the dynamic Smagorinsky models and an alternative hybrid LES–RANS – all computed on the same grid. Data of a highly resolved LES (roughly 13 million cells) are used for reference. Furthermore, the impact of resolution and, therefore, the location of the LES–RANS interface is studied.

1. Introduction

The flow over a periodic arrangement of smoothly contoured hills [16] has been extensively studied over the past few years [4–6,9,11,12,14]. Recently, this flow configuration at $Re_b = 10,595$ was selected as a common test case within the French-German research group on 'Large-Eddy Simulation of Complex Flows'. Originally based on the experiments of Almeida et al. [1], the numerical benchmark case had been modified to be more suitable for numerical simulations [16]. An experiment corresponding to this new setup is presently designed at the University of Technology Munich in order to provide future experimental reference data. New computational reference solutions have been already obtained by the French-German research group [4, 6]. These include highly resolved Large-Eddy Simulation (LES) at $Re_b = 10,595$ using 13×10^6 grid cells and Direct Numerical Simulations (DNS) at $Re_b = 2,800$ and $5,600$.
A detailed analysis of structural characteristics of this flow configuration has revealed a number of interesting features as reported by Fröhlich et al. [9]. The type of flow under consideration is a challenging test case for statistical turbulence models. In various workshops [12,14], Reynolds-averaged Navier-Stokes (RANS) methods failed to predict the reattachment accurately and exhibited a large sensitivity to the individual turbulence closure model. This failure is commonly attributed to the inability of RANS to capture the large-scale dynamics in the separated shear layer. This large-scale motion dominates the momentum exchange and thus determines how quickly the separated flow reattaches. On the other hand, LES is designed to capture these flow structures, but predictions of wall-bounded flows (without wall functions) are limited to moderate Reynolds numbers due to extremely high resolution requirements in the near-wall region. Various hybrid LES–RANS strategies were

[1]Contact: saric@sla.tu-darmstadt.de
[2]Large-Eddy Simulation of Complex Flows (FOR 507) - a French-German Research Group (http://www.hy.bv.tum.de/DFG-CNRS/)

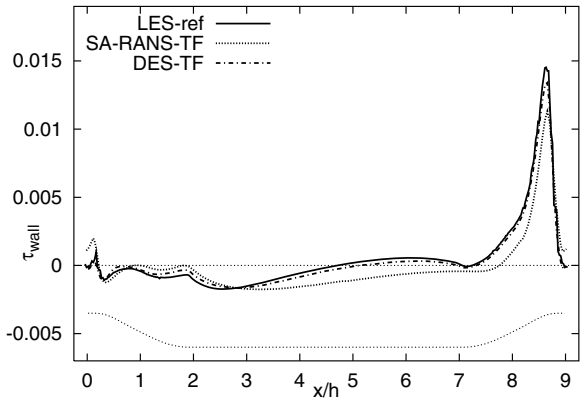

FIGURE 1. LES, DES and 2D SA-RANS predictions of the time-averaged wall shear stress; the hill contour is included for reference.

proposed to alleviate this dilemma. The arguably most popular of these methods is Detached-Eddy Simulation (DES) [17, 20] based on the one-equation Spalart-Allmaras (SA) RANS model [19]. In this approach, the interface between the RANS and LES regions is dictated by the grid design. If performed on a suitable grid, DES are typically expected to yield results superior to those obtained with RANS computations (for the flow investigated in the present study cf. Fig. 1). However, due to its complex grid sensitivity, serious deterioration of the predictions occur if the LES–RANS interface resides at either too far or too close distances to the wall. Noting that the SA model has been tuned for external aerodynamic flows at high Reynolds number, it is interesting to examine DES performance in a complex wall-bounded flow such as the periodic hill configuration. DES has been designed relying on the capability of a RANS model to predict boundary layer flows, and on the superiority of LES in separated flow regions. The hill flow poses yet another challenge for DES: strong spatial and temporal fluctuations of the separation line.

The present work investigates the performance of DES for the hill flow at $Re_b = 10,595$ using computational meshes limited to one million cells – a number feasible for computations on present day personal computers. In order to ensure independence of the findings from numerical methods and particular implementations, several independent research groups computed the same flow by DES using different flow solvers, but employing the same standard grid ($N_x \times N_y \times N_z = 160 \times 100 \times 60$) depicted in Fig. 2. As reference data serve results from a highly resolved LES obtained with roughly 13 million cells [6].

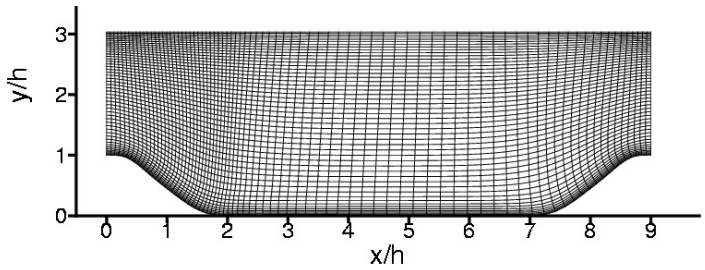

FIGURE 2. A slice of the standard grid ($x - y$ plane, every second grid line shown).

The performance of the DES is further evaluated by comparison of its results to those computed on the same grid using LES with the standard and the dynamic Smagorinsky models and an alternative hybrid LES–RANS proposed by Breuer and Jaffrézic [5] and Jaffrézic et al. [11]. In addition, LES data employing an immersed

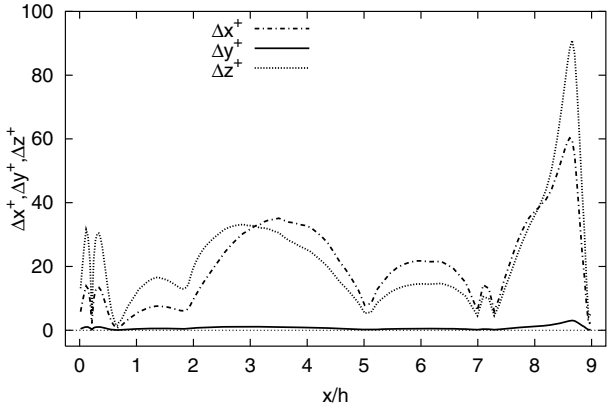

FIGURE 3. Wall-adjacent cell size in wall units along the lower wall boundary for the standard grid.

boundary technique on Cartesian meshes are included. Finally, the impact of resolution and, therefore, the location of the LES–RANS interface is studied.

2. Computational details

A concise description of the flow configuration studied and various flow solvers employed in the present work are outlined first. Afterwards, the main features of the performed simulations will be introduced in order to facilitate the proper analysis and comparison of the results. The Reynolds number, based on the hill height (h) and the bulk velocity above the crest (U_b) is 10,595. The dimensions of the computational domain are $L_x = 9.0h$, $L_y = 3.035h$ and $L_z = 4.5h$.

The choice of the spanwise extent is based on the investigations by Mellen et al. [16]. The flow is assumed to be periodic in the streamwise and spanwise directions, with a no-slip boundary condition applied at both walls. The flow rate is imposed by a spatially constant pressure-forcing term which is adjusted in time to yield the target mass flow rate. The standard grid used in most of the simulations consists of $160 \times 100 \times 60$ cells providing a near-wall resolution in wall units of $\Delta x^+, \Delta z^+ < 35$ in the streamwise and spanwise directions, respectively (see Fig. 3). The values of $\Delta {y_1}^+$ in the near-wall cells do not exceed 1 for most of the computational domain, i.e. for $x/h = 0-8$. The exception is the windward side of the hill, where the resolution decreases. Nevertheless, compared to the values of $\Delta {y_1}^+ = O(1)$, $\Delta x^+ = O(50)$ and $\Delta z^+ = O(20)$, typically recommended for wall-resolved LES, the grid is still deemed to be adequate, although significantly coarser than the grid used in the reference LES (1 vs. 13 million grid cells). This is mainly due to a larger cell size in the spanwise direction that is intentionally chosen such that the RANS region in the framework of DES covers the first 7-9 cells and 4-5 cells in the wall-normal direction at the lower and upper walls, respectively. In some computations even coarser grids are used, being obtained simply by decreasing either the spanwise or the streamwise resolution, while maintaining the original wall-normal cell distribution and uniformity of the cell size in the spanwise direction. These additional simulations with coarser resolutions in the wall-parallel directions are conducted in order to assess the influence of the LES–RANS interface position on the DES performance. Five computer codes, namely LESOCC [2,3], LESOCC2 [10], ISIS [7], FASTEST [8] and MGLET [15,18] are used to predict the periodic hill flow. The first four codes solve the incompressible Navier-Stokes equations on curvilinear block-structured grids by finite-volume methods with collocated arrangement of the Cartesian velocity components. MGLET employs an immersed boundary method on a Cartesian grid. For this grid, $221 \times 173 \times 106$ (4.1 million) cells are used. With this number, the high wall-normal resolution achieved by the curvilinear grid for the other codes could not be reached. At the point of maximum wall shear stress, the wall-adjacent cell size is $\Delta x^+ \approx 11$, $\Delta y^+ \approx 8$ and $\Delta z^+ \approx 56$ leading to a maximum wall-normal distance of about 10 wall units. In all codes, second-order

central differences are used to discretize convective and diffusive terms. An exception concerns the simulations performed with the ISIS code for which the Gamma Differencing Scheme (GDS) is applied for the transport equation for $\tilde{\nu}$, giving a behavior similar to the first-order upwind scheme [13]. With LESOCC2, the HLPA scheme [23] is used for the $\tilde{\nu}-$equation. Different second-order accurate time integrations are employed.
The three-dimensional, incompressible unsteady Navier-Stokes equations, upon filtering read:

$$\frac{\partial \overline{U}_i}{\partial x_i} = 0 \tag{2.1}$$

$$\frac{\partial \overline{U}_i}{\partial t} + \frac{\partial (\overline{U}_i \overline{U}_j)}{\partial x_j} = -\frac{1}{\rho}\frac{\partial \overline{P}}{\partial x_i} + \frac{\partial}{\partial x_j}(\nu \frac{\partial \overline{U}_i}{\partial x_j} - \tau_{ij}) \tag{2.2}$$

where the filter width is determined implicitly by the mesh size. The subgrid scale tensor τ_{ij} is approximated by employing Boussinesq's formulation for the SGS turbulent viscosity, which is modeled using the Smagorinsky formulation:

$$\nu_t = (C_s \Delta)^2 \left|\overline{S}\right|, \qquad \left|\overline{S}\right| = (2\overline{S}_{ij}\overline{S}_{ij})^{1/2} \tag{2.3}$$

with $\Delta = (\Delta x \Delta y \Delta z)^{1/3}$ being a representative measure for the grid spacing, thus approximating the filter width. The model coefficient is either taken as $C_s = 0.1$ along with the van Driest damping function in the near-wall region (the standard Smagorinsky model-SM), or obtained by the dynamic procedure of Germano (the dynamic Smagorinsky model-DSM). In order to stabilize the dynamic model in LESOCC, averaging of the numerator and the denominator in the relation for the determination of the Smagorinsky value is carried out in the spanwise homogeneous direction and also in time using a recursive digital low-pass filter. Additionally, the eddy viscosity is clipped to avoid negative values leading to a destabilization of the numerical scheme.
A one-equation turbulence model by Spalart and Allmaras (SA) [19], is employed to model the influence of the unresolved scales on the resolved ones in the framework of DES [20, 22]. The SA-RANS model determines the modified turbulent viscosity ($\tilde{\nu}$) from the corresponding transport equation, whose destruction term is modeled in terms of the distance to the nearest wall d:

$$\frac{D\tilde{\nu}}{Dt} = C_{b1}\tilde{S}\tilde{\nu} + \frac{1}{\sigma_{\tilde{\nu}}}\left[\frac{\partial}{\partial x_j}\left((\nu + \tilde{\nu})\frac{\partial \tilde{\nu}}{\partial x_j}\right)\right] + \frac{C_{b2}}{\sigma_{\tilde{\nu}}}\left(\frac{\partial \tilde{\nu}}{\partial x_j}\right)^2 - C_{w1} f_w \frac{\tilde{\nu}}{d^2} \tag{2.4}$$

The wall boundary condition is $\tilde{\nu} = 0$ and the standard model constants described in [19] are used. The DES formulation is obtained by replacing the wall distance d by $\tilde{d}$, which is defined as

$$\tilde{d} = \min(d, C_{DES}\Delta_{DES}) \tag{2.5}$$

where a somewhat modified length scale ('DES filter') valid in the 'LES region' of the flow field is introduced as $\Delta_{DES} = max(\Delta x, \Delta y, \Delta z)$. This modification of the destruction term in Eq. (2.4) tunes the model to function in the RANS mode in the near-wall regions ('attached' boundary layers), whereas away from the walls, in the 'detached' regions of the flow, the closure reduces to a (one-equation) Smagorinsky-like model for the SGS eddy-viscosity. The original value of the corresponding model constant of $C_{DES} = 0.65$ is adopted for the current study.

The present work is focussed on DES as the arguably most popular and widely used hybrid LES–RANS method. Another hybrid LES–RANS technique proposed by Breuer and Jaffrézic [5] is tested for comparison. This method employs a one-equation (OE) model based on the transport equation for the turbulent kinetic energy which governs the modeled turbulent kinetic energy k_{mod} in RANS mode and the subgrid scale turbulent kinetic energy k_{sgs} in LES mode. More details about the method and switching criteria defining the LES–RANS interface can be found in [5, 11].
A summary of the simulations performed is given in Table 1 displaying the notation used henceforth, the main parameters and information pertinent to the computations, and the location of separation and reattachment

TABLE 1. Summary of the computations (SJ: Šarić & Jakirlić, code FASTEST; BJ: Breuer & Jaffrézic, code LESOCC, OE-One-Equation model for the turbulent kinetic energy k; DC: Deng & Chikhaoui, code ISIS; TF: von Terzi & Fröhlich, code LESOCC2; PM: Peller & Manhart, code MGLET); t_a: averaging time, t_x: flow-through time, $(\cdot)_s$: separation point, $(\cdot)_r$: reattachment point.

Case	*Grid*	*Model*	$\Delta t U_b/h$	t_a/t_x	$(x/h)_s$	$(x/h)_r$
LES-ref	$281 \times 222 \times 200$	*DSM*	0.0018	141	0.190	4.694
DES-SJ	$160 \times 100 \times 60$	*SA*	0.0105	31	0.214	5.123
DES1-SJ	$160 \times 100 \times 45$	*SA*	0.0105	30	0.214	5.012
DES2-SJ	$160 \times 100 \times 30$	*SA*	0.0105	28	0.214	4.792
LES-SJ	$160 \times 100 \times 30$	*SM*	0.0105	28	0.182	4.902
LES1-BJ	$160 \times 100 \times 60$	*SM*	0.004	69	0.214	4.576
LES2-BJ	$160 \times 100 \times 60$	*DSM*	0.004	71	0.247	4.262
DES-BJ	$160 \times 100 \times 60$	*SA*	0.004	67	0.182	5.235
HYB-BJ	$160 \times 100 \times 60$	*OE*	0.004	65	0.279	4.792
DES-DC	$160 \times 100 \times 60$	*SA*	0.007	200	0.187	5.013
DES1-DC	$80 \times 100 \times 60$	*SA*	0.007	90	0.214	4.957
DES-TF	$160 \times 100 \times 60$	*SA*	0.008	93	0.182	5.123
LES-IB-PM	$221 \times 173 \times 106$	*DSM*	0.004	80	0.270	4.270

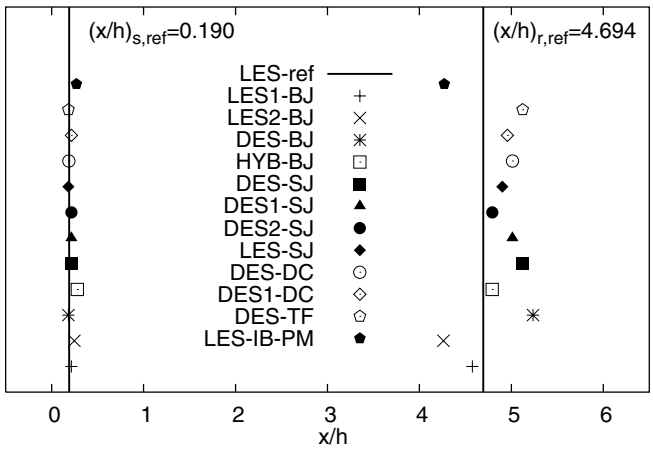

FIGURE 4. Comparison of predicted separation and reattachment locations

points. At this point, one should note that the LES-ref, LES2-BJ and LES-IB-PM computations use the dynamic SM, whereas LES1-BJ and LES-SJ employ the standard Smagorinsky model with the constant $C_s = 0.1$ damped by means of the standard van-Driest damping function. It should also be noted that LES-IB-PM uses no wall model although the wall-normal resolution goes up to 10 wall units.

3. RESULTS

In this section, the performance of DES will be assessed. The Reynolds number of 10,595 is not as high as desirable for testing an hybrid LES–RANS method, but an analysis can only be undertaken relying on highly resolved LES reference data [4, 6] which are not available at higher Reynolds numbers. An important issue for the successful computation of this flow is to accurately capture the separation point [9]. This is achieved

by all applied methods as illustrated in Fig. 4 and Table 1 indicating that the grid resolutions are sufficiently fine for capturing this flow phenomenon. Note that separation and reattachment locations are defined as the locations with zero skin-friction of the mean flow. Deviations in predicted reattachment locations are observed; the majority of the computations predict a delayed reattachment.
Henceforth, profiles of velocities, Reynolds stresses and turbulent kinetic energy are compared to those of the reference LES at the following stations: $x/h = 0.5$, 2, 4, 6 and 8. The selected positions include the regions just upon separation ($x/h = 0.5$), in the middle of the recirculating zone ($x/h = 2$), prior to the reattachment ($x/h = 4$), the post-reattachment and flow recovery ($x/h = 6$), and the region of accelerating flow on the windward slope of the hill.

3.1. **DES on the standard grid using different flow solvers**

First, DES results generated using different flow solvers on the same standard grid are presented. Figs. 5 and 6 show the mean velocity and turbulence statistics.

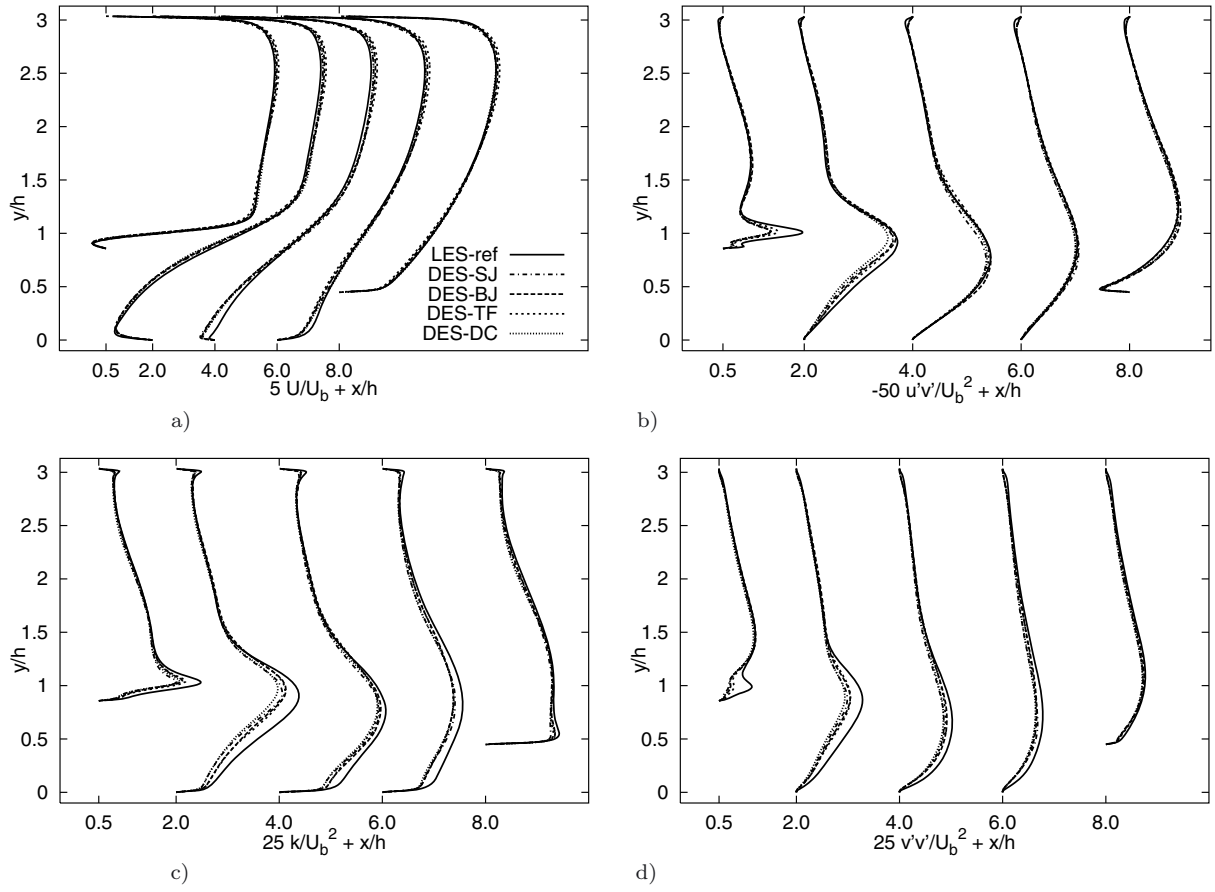

FIGURE 5. Comparison of DES predictions obtained by different codes on the standard grid: a) mean streamvise velocity, b) resolved Reynolds shear stress $\overline{u'v'}$, c) resolved turbulent kinetic energy k, d) resolved normal Reynolds stress $\overline{v'v'}$.

The mean streamwise velocity profiles exhibit good agreement with the reference data at positions $x/h = 0.5$, 2 and 8, whereas discrepancies are observed in the regions prior and after flow reattachment (at locations $x/h = 4$

and 6). Here, the backflow velocity ($x/h = 4$) is overpredicted corresponding to longer reattachment and slower recovery farther downstream (Fig. 5a). Despite the good agreement of the Reynolds shear stresses (Fig. 5b), DES results yield insufficient turbulent kinetic energy within the reattachment region (Fig. 5c). Furthermore, the near-wall peak of the wall-normal Reynolds stress $\overline{v'v'}$ at $x/h = 0.5$ cannot be captured accurately by DES, which has an impact on the results farther downstream (see Fig. 5d). One possible reason for this behavior could be that the 'DES filter' $\Delta = \max(\Delta x, \Delta y, \Delta z)$ in this region is 40% larger than the one employed by LES $\Delta = (\Delta x \Delta y \Delta z)^{1/3}$ on the same grid. Hence, the SGS-viscosity of DES is larger in this flow region.

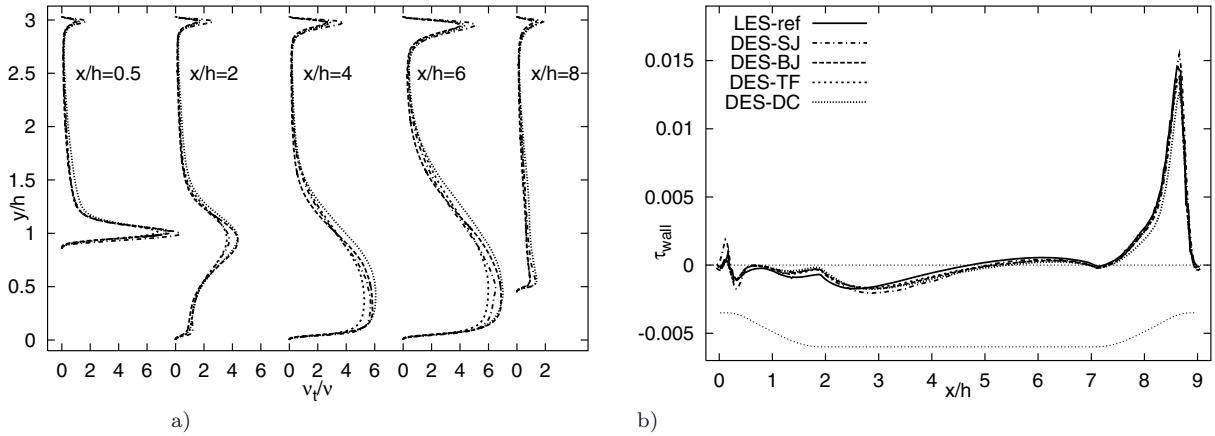

FIGURE 6. Comparison of DES predictions obtained by different codes on the standard grid: a) time-averaged turbulent viscosity and b) time-averaged wall shear stress distribution on the lower wall.

Code dependency, on the other hand, can be ruled out, since different flow solvers with distinct implementations and various numerical methods predict the same flow behavior on the same grid. However, minor discrepancies in the results remain owing to differences in numerical methods and chosen time steps. Slight deviations in the mean flow and predictions of turbulence statistics originate from differences in the computed turbulent viscosity as shown in Fig. 6a. The profiles of the wall shear stress on the lower wall agree reasonably well with the reference data (Fig. 6b), but they reveal that the DES consistently underpredict the wall shear stress in the reattachment region and consequently yield a delayed reattachment. Overall, the mutual agreement of the independently performed DES is very good, thus demonstrating a high level of fidelity of the results.

3.2. **Influence of the turbulence modeling strategy**

In order to investigate the influence of the turbulence modeling, i.e. applied simulation strategies, profiles of the mean streamwise velocity along with the (resolved) Reynolds shear stresses obtained with different approaches are compared in Fig. 7. All results in this figure are obtained with the same code (LESOCC) on the standard grid. The mean velocity profiles displayed in Fig. 7a exhibit a similar good behavior of both hybrid LES–RANS computations DES-BJ and HYB-BJ, but also a surprising deficiency of the dynamic LES (LES2-BJ) in this simulation, which will be discussed below.

Concerning HYB-BJ and DES-BJ, despite the discrepancy at the location $x/h = 4$ already mentioned for all the previously commented DES, the mean streamwise velocity is in good agreement with the reference LES. It is noticeable that HYB-BJ captures the reattachment point accurately and better than DES-BJ (see Fig. 4). One can see that the hybrid simulation HYB-BJ fails to capture the tiny separation at the hill crest (see Fig. 8). This kind of behavior of the wall shear stress has already been observed in RANS simulations as illustrated in Fig. 1. A detailed evaluation of this hybrid approach can be found in [11]. Almost excellent predictions of

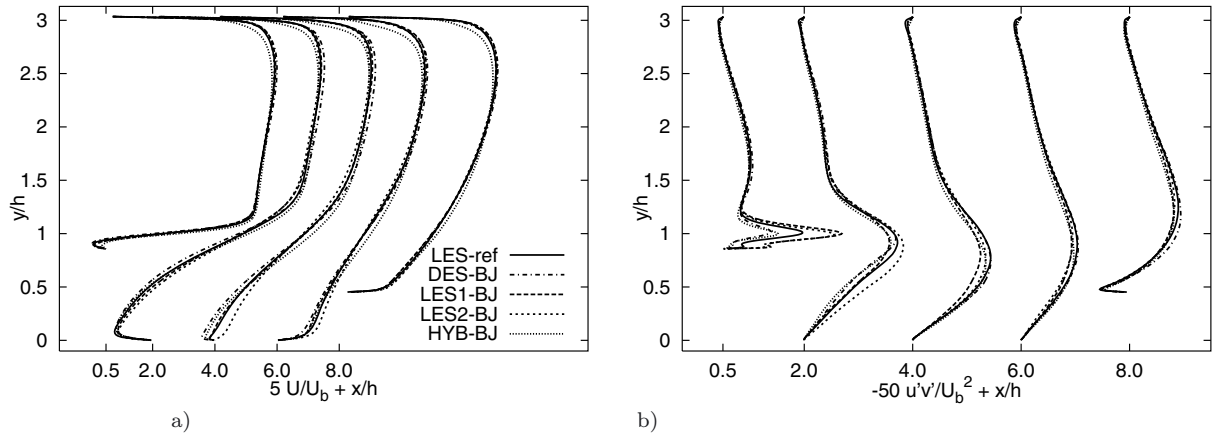

FIGURE 7. Influence of turbulence modeling/simulation strategies on the hill flow predictions on the same grid: a) mean streamvise velocity, b) resolved Reynolds shear stress $\overline{u'v'}$.

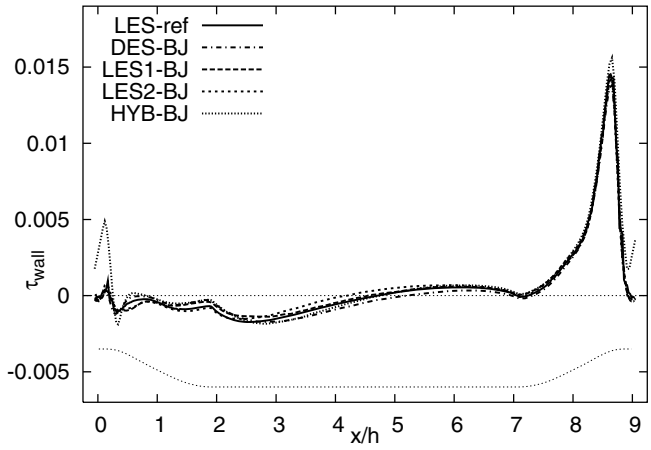

FIGURE 8. Time-averaged wall shear stress distributions on the lower wall predicted by different models.

the mean streamwise velocity profiles obtained by LES employing the standard SM are evident. This supports the previous assertion that the grid resolution is deemed to be adequate, with the exception of the region of separated shear layer (see Fig. 7b at $x/h = 0.5$) where shear stress overpredictions associated with a locally coarser grid are visible. At the same time, the results reveal surprisingly poor performance of the dynamic SM. This is demonstrated by the wall shear stress distribution plotted in Fig. 8 which shows the dynamic SM predicting too short a recirculation zone. This unexpected behavior is an indication of high grid sensitivity of the dynamic SM, which is confirmed by direct comparison of various LES computations presented in Figs. 9 and 10 all applying DSM. The simulation LES-IB-PM using the immersed boundary method was performed with 4.1 million grid cells. The computational effort of the additional cells is more than compensated by a substantially lower cost per grid point. Therefore, the increase in number of grid points with this method is justified for a fair comparison. However, due to the use of a Cartesian grid, the wall-normal resolution was substantially coarser than in the curvilinear grid used for the other simulations. Differences with respect to LES2-BJ are clearly noticeable in the profiles of the mean streamwise velocity and shear stress. In particular,

LES-IB-PM yields better velocity predictions (Fig. 9a). The wall shear stress distribution shown in Fig. 10 reveals that despite close agreement within the recirculation zone, these two simulations generate different wall shear stresses elsewhere. LES-IB-PM fails to capture both the tiny separation at the hill crest and the small recirculation region just before the windward side of the hill. These deviations between the two LES predictions using the dynamic SM can be attributed to the different grids and boundary treatments employed, whereas the discrepancies between the standard (LES1-BJ) and dynamic SM (LES2-BJ) using the same code and grid can be imputed to a higher SGS eddy-viscosity prediction of LES2-BJ in comparison to LES1-BJ.

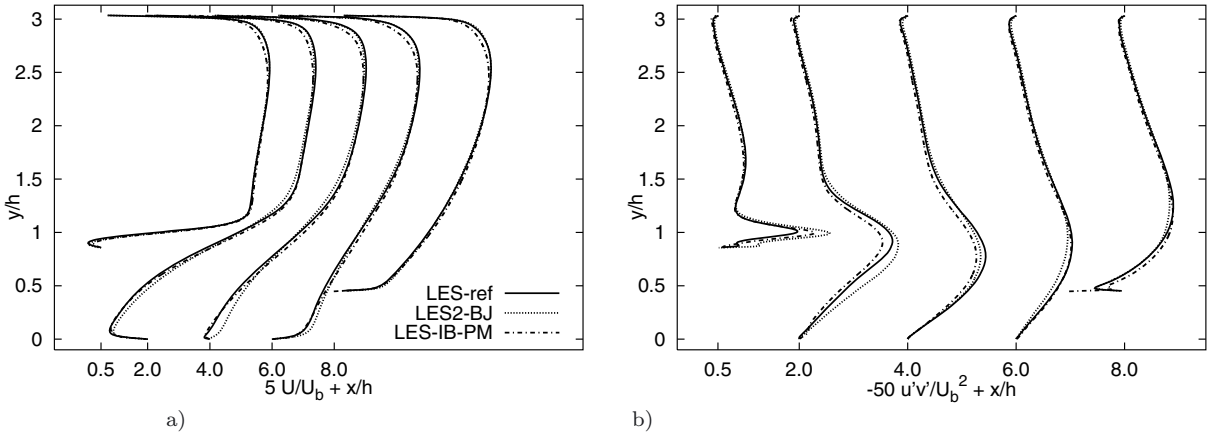

FIGURE 9. Comparison of LES results obtained by different codes: a) mean streamwise velocity, b) resolved Reynolds shear stress $\overline{u'v'}$.

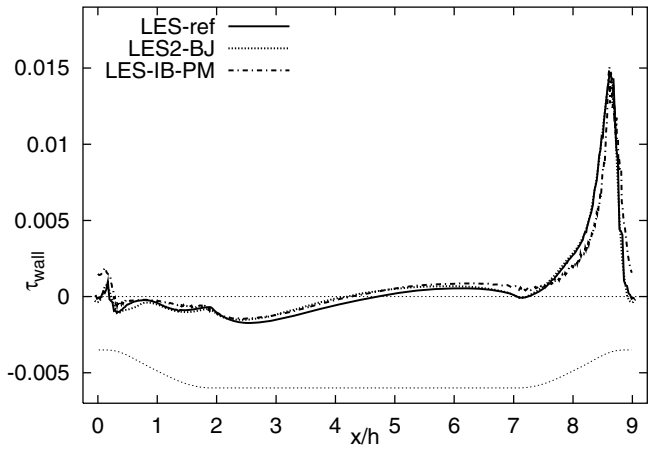

FIGURE 10. Time-averaged wall shear stress distributions on the lower wall for LES obtained by different codes.

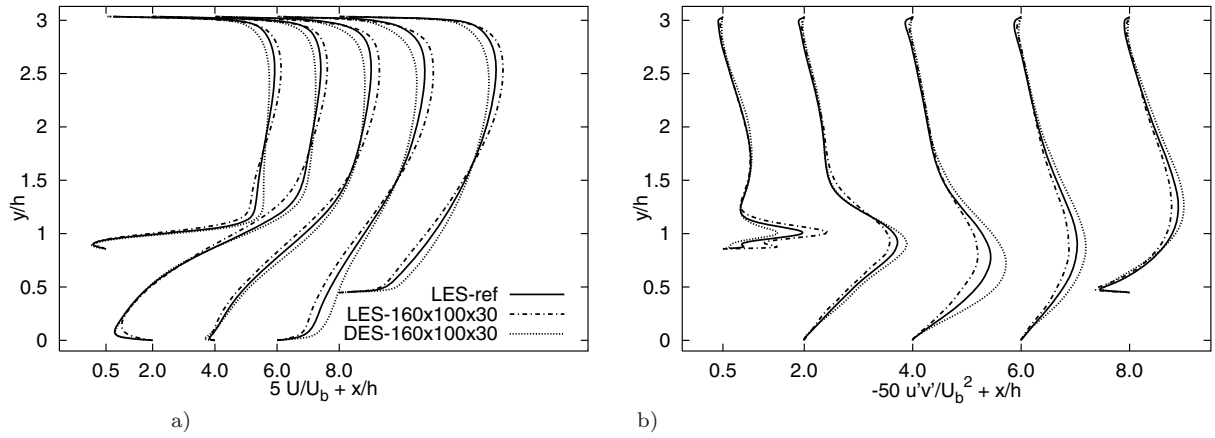

FIGURE 11. DES vs. LES on the same coarse grid: LES-SJ and DES-SJ. a) mean streamvise velocity, b) resolved Reynolds shear stress $\overline{u'v'}$.

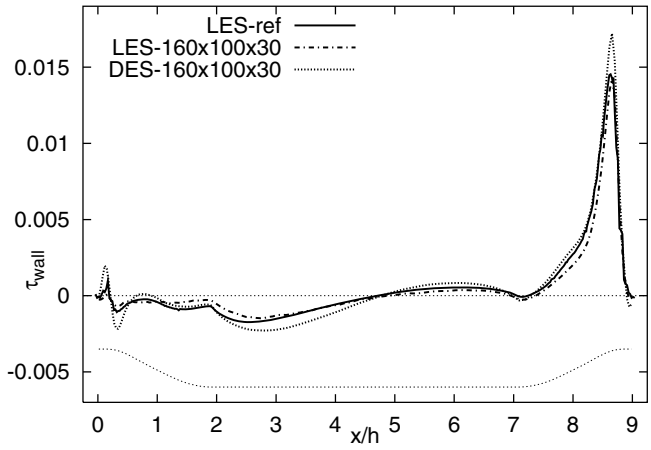

FIGURE 12. Time-averaged wall shear stress distributions on the lower wall: DES vs. LES on the same grid.

3.3. **DES vs. LES on a coarser grid**

Comparable deviations from the reference solution for LES and DES on the standard grid have been demonstrated in the previous section. The two methods are further compared directly by additional simulations conducted on the same, but two times coarser grid in spanwise direction (DES2-SJ, LES-SJ). Indeed the purpose of the hybrid LES–RANS strategies is to decrease the near-wall resolution in the streamwise and spanwise directions, for which LES is assumed to fail. Profiles of the mean streamwise velocity, Reynolds shear stress and wall shear stress are compared in Figs. 11 and 12.

Still, the results of DES are comparable to LES and no evident superiority of DES is observed. This tends to prove that the grid resolution is still sufficient for LES to predict reasonably well separation and reattachment. Temmerman et al. [21] have also obtained separation and reattachment points at x/h =0.23 and 4.64, respectively, by LES using $N_x \times N_y \times N_z = 112 \times 64 \times 56$ cells. Hence, the considered grids are 'not coarse enough'. One could assume that for higher Reynolds numbers this might not be the case any more and DES

might finally achieve significant advantages over LES on the same coarse grid. This assertion, however, still awaits corroboration.

3.4. **Influence of the LES–RANS interface location**

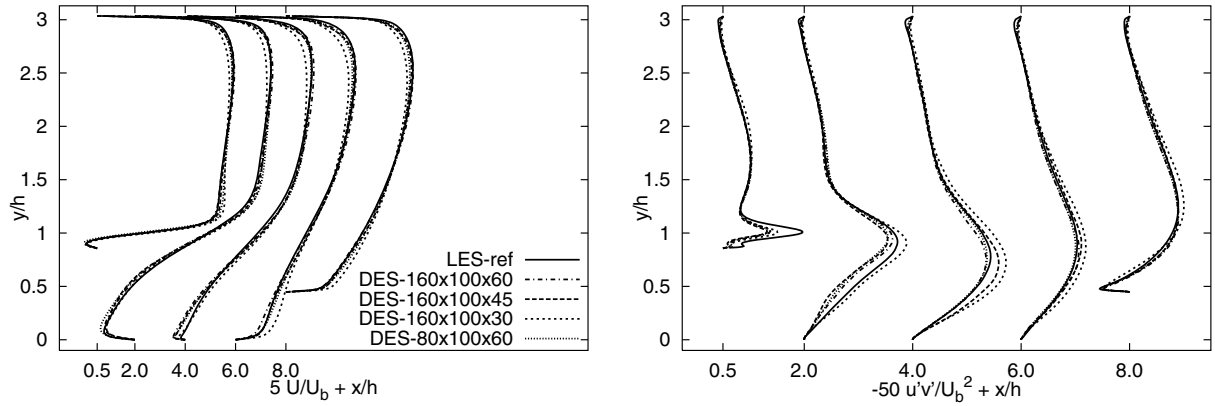

a) b)

FIGURE 13. Influence of grid resolution on DES: a) mean streamwise velocity, b) resolved Reynolds shear stress $\overline{u'v'}$.

Finally, the influence of the position of the LES–RANS interface on the performance of DES is investigated. For this purpose, coarser grids are generated simply by decreasing the spanwise resolution of the standard grid. An additional configuration is created by removing every second grid point in the streamwise direction (grid: $80 \times 100 \times 60$). In both cases the original wall-normal cell distribution is intentionally maintained to provide different positions of the LES–RANS interface which is dictated by grid design. Fig. 13 displays profiles of the mean streamwise velocity and Reynolds shear stress obtained for different DES. No significant differences between the results are observed except for the computation DES2-SJ which predicts an earlier reattachment. However, overpredictions of the shear stresses and a too fast recovery of the boundary layer are observed

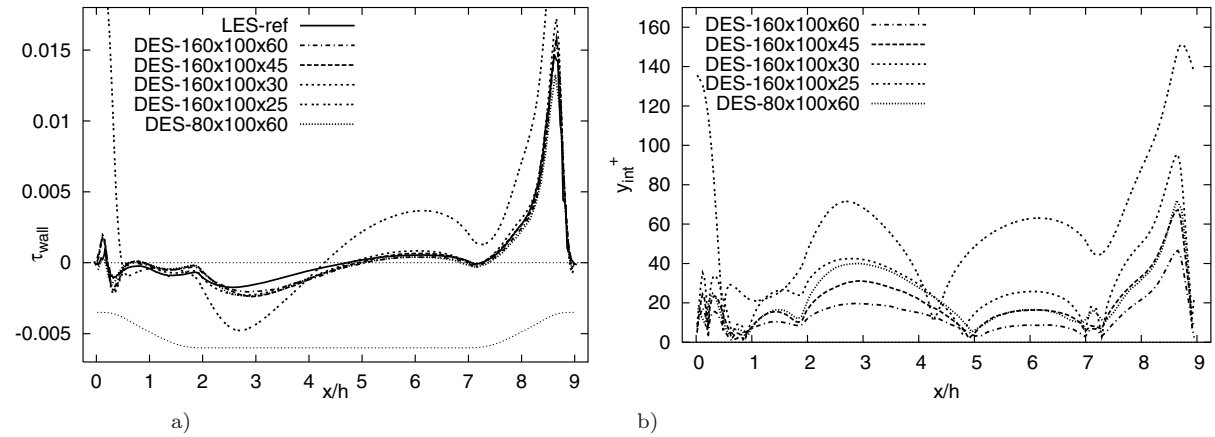

a) b)

FIGURE 14. DES with different grids and locations of the interface. a) time-averaged wall shear stress distributions on the lower wall, b) position of the LES–RANS interface.

downstream of reattachment. Results of DES on an even coarser mesh containing only 25 spanwise cells are included in Fig. 14 showing the wall shear stress distribution and the positions of the LES–RANS interface for the corresponding computations. As the number of spanwise cells is decreased from 60 down to 45 and 30, the position of the LES–RANS interface shifts away from the wall as depicted in Fig. 14b. Predictions of the wall shear stress are consistently deteriorating, but only within the range of $x/h = 0 - 0.5$, whereas the separation point is still captured reasonably well. As the number of spanwise cells is ultimately decreased from 30 to 25, the profile changes dramatically, resulting in extremely poor predictions. This is explained by the LES–RANS interface position which is now beyond the (time-averaged) boundary layer thickness of $\delta \approx 0.1h$ at this location. Hence, for 25 grid cells in the spanwise direction, i.e., an LES–RANS interface at 0.117 h, DES is clearly used outside its intended framework.

4. Conclusions

Detached Eddy Simulations were scrutinized for predicting turbulent channel flow with periodic hill constrictions at a Reynolds number of 10,595 based on bulk velocity and height of the hills. Different flow solvers were used by independent research groups to establish independence of the results from numerical methods and particular implementations. The DES data was compared to results obtained using a highly resolved LES. While discrepancies to the reference data were observed, the DES performed overall well considering the coarse grid. However, for the flow configuration chosen for the present investigation, LES or an alternative hybrid LES–RANS method yielded results of similar quality. Further coarsening of the grid did not alter the performance of DES substantially unless the interface between LES and RANS mode moves outside the boundary layer on the crest of the hill, deteriorating the results substantially.

Acknowledgements

The present research is supported by the Deutsche Forschungsgemeinschaft (DFG) and Centre national de la recherche scientifique (CNRS) through the French-German programme 'LES of complex flows' (FOR 507). The authors thank Centre International des Rencontres Mathématiques (CIRM), Marseille for its hospitality during CEMRACS 2005.

References

[1] Almeida, G.P., Heitor, M.V. (1993): *Wake Flows behind Two-Dimensional Model Hills*, Expl. Thermal Fluid Sci., **7**, pp. 87-101.

[2] Breuer, M., Rodi, W. (1996): *Large-Eddy Simulation of Complex Turbulent Flows of Practical Interest*, Vieweg, In: Flow Simulation with High-Performance Computers II, Notes on Numer. Fluid Mech., vol. **52**, pp. 258–274

[3] Breuer, M. (1998): *Large-Eddy Simulation of the Sub-Critical Flow Past a Circular Cylinder: Numerical and Modeling Aspects,* Int. J. Num. Methods Fluids, vol. **28**, pp. 1281–1302

[4] Breuer, M., Jaffrézic, B., Manhart, M., Peller, N., Fröhlich, J., Hinterberger, C., Rodi, W., Deng, G., Chikhaoui, O., Šarić, S., Jakirlić, S. (2005): *A Comparative Study of the Turbulent Flow over a Periodic Arrangement of Smoothly Contoured Hills*, 6^{th} ERCOFTAC Workshop on Direct and Large-Eddy Simulation: DLES-6, September 12-14, 2005, Poitiers, France.

[5] Breuer, M., Jaffrézic, B. (2005): *Hybrid LES–RANS Technique Based on a One-Equation Near-Wall Model*, EUROMECH Colloquium 469, *Large-Eddy Simulation of Complex Flows*, October 6-8, 2005, Dresden, Germany.

[6] Breuer, M. (2005): *New Reference Data for the Hill Flow Test Case*, personal communication, `http://www.hy.bv.tum.de/DFG-CNRS/`

[7] Deng, G.B., Queutey, P., Visonneau, M. (2005): *Three-Dimensional Flow Computation with Reynolds Stress and Algebraic Stress Models*, In: Engineering Turbulence Modelling and Experiments 6, ed. W. Rodi and M. Mulas, ELSEVIER, pp. 389–398

[8] Durst, F., Schäfer, M. (1996) *A Parallel Block–Structured Multigrid Method for the Prediction of Incompressible Flows*, Int. J. Num. Methods Fluids, vol. **22**, pp. 549–565.

[9] Fröhlich, J., Mellen, C.P., Rodi, W., Temmerman, L., Leschziner, M.A. (2005): *Highly Resolved Large-Eddy Simulation of Separated Flow in a Channel with Streamwise Periodic Constrictions*, J. Fluid Mech., **526**, pp. 19-66.

[10] Hinterberger, C. (2004): *Dreidimensionale und tiefengemittelte Large-Eddy-Simulation von Flachwasserströmungen*, Ph.D. Thesis, University of Karlsruhe.

[11] Jaffrézic, B., Breuer, M., Chikhaoui, O., Deng, G., Visonneau, M. (2006): *Towards Hybrid LES–RANS-Coupling for Complex Flows with Separation*, CEMRACS 2005 Proceedings, August-September, 2005, Marseille, France.

[12] Jakirlić, S., Jester-Zürker, R., Tropea, C. (2002): *Report on 9th ERCOFTAC/IAHR/COST Workshop on Refined Turbulence Modelling*, October, 9-10, 2001, Darmstadt University of Technology, ERCOFTAC Bulletin, No. **55**, pp. 36-43.

[13] Jasak, H. (1996): *Error Analysis and Estimation for the Finite Volume Method with Applications to Fluid Flows*, Ph.D. Thesis, University of London.

[14] Manceau, R., Bonnet, J.-P., Leschziner, M.A., Menter, F. (eds.) (2002): *10th Joint ERCOFTAC(SIG-15)/IAHR/QNET-CFD Workshop on Refined Flow Modelling*, Université de Poitiers, France, October, 10-11, 2002.

[15] Manhart, M. (2004): *A Zonal Grid Algorithm for DNS of Turbulent Boundary Layers,* Computers and Fluids, 33(3):435–461.

[16] Mellen, C.P, Fröhlich, J., Rodi, W. (2000): *Large-Eddy Simulation of the Flow over Periodic Hills*, Proceedings of 16^{th} IMACS World Congress, Lausanne, Switzerland, 2000, (eds.) Deville, M., Owens, R.

[17] Nikitin, N.V., Nicoud, F., Wasistho, B., Squires, K.D., Spalart, P.R. (2000): *An Approach to Wall Modelling in Large-Eddy Simulations*, Phys. Fluids, **12**/7, pp. 1629-1632.

[18] Peller, N., Le-Duc, A., Tremblay, F. and Manhart, M. (2006): *High-order Stable Interpolations for Immersed Boundary Methods*, International Journal for Numerical Methods in Fluids, in press.

[19] Spalart, P.R., Allmaras, S.R. (1994): *A One-Equation Turbulence Model for Aerodynamic Flows*, La Rech. Aérospatiale, **1**, pp. 5-21.

[20] Spalart, P.R., Jou, W.-H., Strelets, M., Allmaras, S. R. (1997): *Comments on the Feasibility of LES for Wings, and on a Hybrid RANS/LES Approach*, Advances in DNS/LES, 1st AFOSR Int. Conf. on DNS/LES, Aug 4-8, 1997, Greyden Press, Columbus, OH.

[21] Temmerman, L., Hadžiabdić, M, Leschziner, M.A., Hanjalić, K. (2005): *A Hybrid Two-Layer URANS-LES Approach for Large-Eddy Simulation at High Reynolds Numbers*, Int. Journal of Heat and Fluid Flow, **26**, pp. 173-190.

[22] Travin, A., Shur, M., Strelets, M., and Spalart, P.R. (2002): *Physical and Numerical Upgrades in the Detached-Eddy Simulation of Complex Turbulence Flows*, In: Fluid Mechanics and Its Application: Advances in LES of Complex Flows.

[23] Zhu, J., Rodi, W. (1991): *A low dispersion and bounded conveciton scheme*, Comput. Meth. Appl. Mech. Eng., **92**, pp. 87-96.